GEOPHYSICS, VOL. 69, NO. 3 (MAY-JUNE 2004); P. 762–771, 6 FIGS., 1 TABLE.
10.1190/1.1759462

Induced polarization measurements on unsaturated, unconsolidated sands

Craig Ulrich* and Lee D. Slater*

ABSTRACT

Induced polarization (IP) measurements were obtained on unsaturated, unconsolidated sediments during (1) evaporative drying and (2) pressure drainage followed by subsequent imbibition (water reentry). Porous ceramic discs were used with existing laboratory IP instrumentation to permit accurate IP measurements on unsaturated samples. Polarization magnitude during evaporative drying approximates a power law dependence on saturation. Saturation exponents for the polarization term were consistently less than Archie conduction exponents, although no clear relationship between the exponents was observed. The polarization measured over a pressure drainage and imbibition cycle exhibits a complex (yet similar between tested samples) saturation dependence, being a function of saturation range and saturation history. Polarization is observed to increase with saturation over certain saturation intervals, yet decrease with saturation over others. High polarization observed during sample imbibition is consistent with a model for the development of a continuous charged air-fluid interface as previously proposed to explain hysteresis in resistivity measurements. The saturation dependence of the phase angle measured in IP in large part results from changes in conduction as pores fill and drain. Models of low-frequency polarization based on grain-size-controlled and pore-size-controlled relaxation both support dependence of IP measurements on saturation. Our results suggest that saturation dependent polarization must be considered for effective interpretation of IP measurements from the vadose zone.

INTRODUCTION

The growing interest in the application of the induced polarization (IP) method in environmental investigations results from recent studies that illustrate the sensitivity of IP parameters to important lithologic parameters, including surface area, grain size and hydraulic conductivity (e.g., Börner et al., 1996; Slater and Lesmes, 2002). However, published studies considering the dependence of IP parameters on saturation are sparse (Vinegar and Waxman, 1984; Worthington and Collar, 1984) and models for IP mechanisms in earth materials primarily focus on saturated materials. Consequently, application of the IP method in vadose zone studies has received minimal attention in the recent literature. This also presumably reflects the fact that water content and water distribution are primarily studied with ground-penetrating radar (GPR) or electrical resistivity, and are generally not considered properties of interest in IP exploration. However, knowing the dependence of IP parameters on saturation is clearly necessary in order to reliably interpret IP measurements in terms of lithologic parameters such as grain size, specific surface area, and hydraulic conductivity when the survey is wholly or partly conducted in the vadose zone. Accurate geophysical estimation of vadose zone lithology could enhance development of minimally invasive procedures to determine the distribution of soil moisture content or unsaturated hydraulic conductivity as surface area and grain size exert a primary control on these vadoze zone parameters. We thus recognize a need for studies of IP parameters as a function of saturation in near-surface soils and sediments.

Subsurface polarization results from the presence of interfaces at which local charge concentration gradients develop upon application of electric current. Polarization is enhanced at interfaces associated with metals and clays (see, for review, Ward, 1990; Schön, 1996), but it is also significant and measurable in clay-free and metal-free sediments (Vanhala and Soininen, 1995; Schön, 1996; Vanhala, 1997) where it is associated with predominantly tangential ion displacement in the electrical double layer (EDL) forming at the grain-fluid interface (Lima and Sharma, 1992; Schön, 1996; Börner et al., 1996; Chelidze and Gueguen, 1999; Lesmes and Morgan, 2001). Ionic mobility contrasts at interfaces between wide and narrow pores are also considered a source of polarization enhancement in sandy sediments (Titov et al. 2002).

Electrical parameters in metal-free rocks and sediments are related to the physicochemical properties of the grain surface–fluid interface (e.g., Vinegar and Waxman, 1984; Börner et al.,

Manuscript received by the Editor July 25, 2003; revised manuscript received February 17, 2004.
*Rutgers University, Department of Earth & Environmental Sciences, 195 University Avenue, Room 407, Newark, New Jersey 07102. E-mail: lslater@antromeda.rutgers.edu.

1996; Lesmes and Frye, 2001, Slater and Lesmes, 2002). Surface conduction and polarization at this interface is a function of surface area, surface charge density, surface ionic mobility, and surface tortuosity (Schön, 1996; Revil and Glover, 1998; Lesmes and Frye, 2001). The imaginary conductivity (σ'') measured with IP shows a near-linear correlation with surface area (e.g., Börner and Schön, 1991; Schön, 1996) and an inverse correlation with grain size (e.g., Slater and Lesmes, 2002) in unconsolidated sediments and sandstone. Laboratory studies show that electrolyte chemistry exerts a relatively weak control on surface conduction and polarization of the grain-fluid interface when considering the limited range of electrolyte concentration encountered in most sediments (Vinegar and Waxman, 1984; Revil and Glover, 1998; Lesmes and Frye, 2001). Consequently, IP appears a promising tool for lithologic mapping in near-surface sediments, and the correlation between polarization and surface area/grain size encourages hydraulic conductivity prediction from IP measurements (Börner et al, 1996; Lima and Niwas, 2000; Slater and Lesmes, 2002).

Most IP models generally consider water-saturated samples and neglect to include a saturation term. Chelidze and Guegen (1999) review available theoretical models for the electrical response of porous rocks over a wide frequency range and discuss how percolation models and Maxwell-Wagner-Bruggeman-Hanei (MWBH) type models predict saturation dependence. However, models based on grain-fluid interface polarization are required to predict the low-frequency electrical response of unsaturated earth materials. Vinegar and Waxman (1984) incorporated water:oil saturation into an IP model for shaly sandstone based on the membrane polarization mechanism. Polarization was theoretically and experimentally shown to display power-law saturation dependence, with the imaginary conductivity saturation exponent (p) equal to $n-1$. Worthington and Collar (1984) also present results on sandstone as a function of water:oil saturation in a paper addressing IP parameters and petrophysical properties. Knight and Nur (1987a) investigated the dielectric properties of rocks as a function of saturation in the kilohertz frequency range and related the high apparent dielectric constants observed to interfacial polarization mechanisms. Su et al. (2000) examine the spectral electrical response of rocks as a function of saturation during oil-driving water tests using a two-electrode measurement technique. They found the imaginary conductivity to show a near linear relationship with water:oil saturation in the kilohertz range. Electrode polarization below the kilohertz frequency range, coupled with the potential existence of multiple polarization mechanisms across the full frequency spectrum, limits evaluation of the significance of these measurements on IP surveys.

Uncertainty exists regarding the length scale controlling the EDL polarization observed in rocks and sediments, casting uncertainty on the likely dependence of IP on saturation. Some workers argue theoretically and show experimentally that the dominant relaxation time of the polarization is controlled by the grain size as depicted in Figure 1a (e.g., Klein and Sill, 1982; Lima and Sharma, 1992; Garrouch, 1999; Chelidze and Guegen, 1999; Lesmes and Morgan, 2001). Scott and Barker (2003) present experimental data suggesting that the relaxation is primarily associated with localized charge blockage caused by constrictions in the fluid-filled pore space, linking the IP response to a dominant pore throat size (Figure 1b). Similarly, Titov et al. (2002) formulate a model in terms of interfaces between ion-selective pore-throats and larger pores, again relating the IP mechanism to pore-throat size. Lima and Niwas (2002) choose to recognize the existence of polarization lengths associated with both the grain size and the pore size. Obviously, pore/pore-throat–controlled polarization implies saturation dependent IP parameters whereas saturation dependent IP is less intuitive when considering grain-size–controlled polarization.

Complex electrical measurements on unsaturated water:air materials in the frequency range of IP surveys are poorly documented in the current literature. Kemna (2000), referring to work published in German (Schopper et al., 1997), reports that σ'' showed $n-1$ saturation dependence for measurements on unconsolidated sediments. Slater and Glaser (2003) briefly considered saturation as part of a paper addressing the range of controls on IP in unconsolidated sediments. In this current paper, we report the results of laboratory IP measurements on sandy unconsolidated samples as a function of water content and saturation history. We show how IP parameters vary with saturation and illustrate the existence of hysteresis in both the electrolytic conduction and polarization terms. We also describe the instrumentation and calibration procedure used to obtain reliable IP measurements on unsaturated samples. We discuss the results in terms of (1) polarization mechanisms in unsaturated sediments and (2) interpretation of IP measurements from the vadose zone.

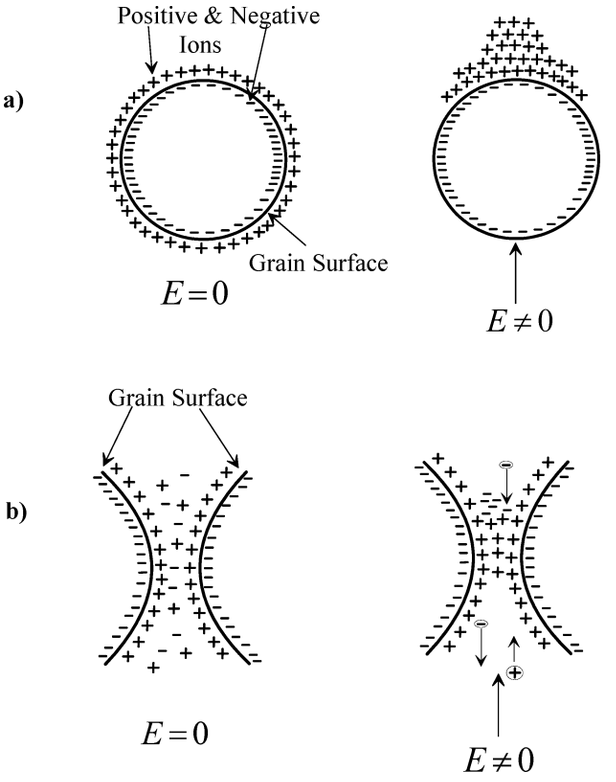

Figure 1. Identified relaxation length scales for EDL polarization in rocks and soils: (a) grain-size–controlled length scale, (b) pore-throat-size–controlled length scale. E denotes electric field.

ELECTRICAL PROPERTIES

The frequency (ω) dependent electrical response of soils in the laboratory is measured in this study using an impedance analyzer. Impedance magnitude and phase shift (ϕ) of the sample are recorded relative to a precision reference resistor upon stimulus with a sine wave. Results may be presented in terms of magnitude and phase or in terms of real and imaginary components of the impedance. It is a matter of choice whether to present measurements in terms of sample impedance or in terms of resistivity, conductivity, or dielectric permittivity, all being calculable from the measured impedance and sample geometry. It is important to note that each of these parameters contains a total energy storage term and a total energy loss term (see Knight and Endres, 2003).

We choose to compute complex conductivity (σ^*). The in-phase (real, σ') conductivity component represents ohmic conduction currents (energy loss), whereas the out-of-phase (imaginary, σ'') conductivity represents the much smaller polarization (energy storage) term. The measured magnitude ($|\sigma|$) and phase (ϕ) parameters are related to the real and imaginary components as follows:

$$|\sigma| = \sqrt{(\sigma'^2 + \sigma''^2)}, \tag{1}$$

$$\phi = \tan^{-1}\left[\frac{\sigma''}{\sigma'}\right] \approx \left[\frac{\sigma''}{\sigma'}\right] (\phi < 100 \text{ mrads}). \tag{2}$$

The phase angle measured in IP defines the ratio of the polarization to the conduction.

Ohmic conduction in nonmetallic rocks is ionic, occurring through the pore-filled electrolyte and by ion migration in the EDL forming at the grain-fluid interface. A common assumption is that the electrolytic conductivity (σ_{el}) and surface conductivity (σ'_{surf}) add in parallel (e.g., Waxman and Smits, 1968; Vinegar and Waxman, 1984):

$$\sigma' = \sigma_{el} + \sigma'_{surf}. \tag{3}$$

The relative importance of σ'_{surf} is critically dependent on matrix mineralogy, grain size, and fluid conductivity (σ_w). In coarse, clay-free sediments saturated with saline groundwater, $\sigma_{el} \gg \sigma'_{surf}$, and Archie's (1942) equations can be used to predict σ' as a function of σ_w, formation factor (F), and saturation (S_w):

$$\sigma' \cong \sigma_{el} = \frac{1}{F}\sigma_w S_w^n = \sigma'_{sat} S_w^n, \tag{4}$$

where σ'_{sat} is the saturated real electrolyte conductivity and n is the saturation exponent related to the distribution of fluid within the pore space. The saturation exponent is a function of the range of saturation studied (e.g., Longeron et al., 1989; Knight, 1991). Hysteresis in the σ_{el} versus S_w relationship results in saturation exponents that differ for drainage versus imbibition (water reentry) curves (Longeron et al., 1989; Knight, 1991).

EXPERIMENTAL PROCEDURE

Four electrode measurements (0.1–1000 Hz) were made using a National Instruments (NI) 4551 Dynamic Signal Analyzer (DSA). Pre-amplification is used to increase the input impedance to approximately $10^9\Omega$ on the sample channel, minimizing errors from the instrumentation. Nonpolarizing (Ag-AgCl) electrodes are used to measure the phase shift (ϕ) and conductivity magnitude ($|\sigma|$) across the sample relative to a reference resistor. All measurements are made in an environmental chamber at $24.5 \pm 0.5^\circ$C. Slater and Lesmes (2002) provide further details of the instrumentation and calibration procedures employed to ensure accurate IP measurements across the investigated frequency range.

In the present study, considerable effort focused on the design of a sample holder that would permit accurate IP measurements of unsaturated, unconsolidated samples. A problem results from the need to maintain electrical contact with an unsaturated sample at the nonpolarizing potential electrodes. One approach is to maximize the surface area of metal electrode in direct electrical contact with the sample. However, placement of metal potential electrodes inside the sample holder and between the current electrode rings produces phase artifacts that increase if the potential electrode is inclined from perpendicular to the primary current flux along the sample (Vanhala and Soininen, 1995). Phase artifacts are minimized when the electrodes make electrical contact with the sample via emplacement in electrolyte-filled chambers built onto the sides of the sample holder (e.g., Lesmes, 1993). We routinely use this approach for saturated samples (e.g., Slater and Lesmes, 2002).

Calibration measurements on water samples of known phase response (0.1–1000 Hz) illustrate the unacceptable phase errors that arise when coil or even small wire electrodes are placed inside the sample and between the current electrodes. Figure 2 shows the phase measured for a water sample of conductivity 395 μS/cm using four measurement geometries. The solid line shows the theoretical phase response of a water sample assuming a relative dielectric permittivity of 81. Coiled potential electrodes placed inside the sample result in anomalous negative phase (configuration 1 in Figure 2). Anomalous phase results are also obtainable when wire electrodes are inside the sample (configuration 2 in Figure 2). Placing the potential electrodes in fluid-filled chambers on the edge of the sample removes such phase errors (configuration 3 in Figure 2). The electrical response of unsaturated soils can be measured with this configuration by using a sealed porous disc with high air entry pressure ($\approx$16 psi) placed in between the potential electrode chamber and the sample holder. Residual 1–2 mrad errors can still arise and depend on the separation between current and potential electrodes. These errors increase with decreasing potential-current electrode separation (compare geometry 3-1 with geometry 3-2 in Figure 2). The sample holder used for all measurements in this study has a phase error $\leq$0.5 mrad across the entire frequency range (geometry 3-2 in Figure 2). We note that poor sample design can result in both capacitive and inductive (negative phase in conductivity space) artifacts.

Unconsolidated sediments were available from samples of the Kansas River floodplain. Laser particle-size analysis was used to determine the grain-size distribution for all samples. The samples are predominantly well-sorted sands with a negligible percentage of clay-size grains. Specific surface area was measured using the nitrogen BET method. Total porosity (ϕ_{tot}), likely to be close to effective porosity (ϕ_{eff}) in these loosely packed sediments, was determined from wet and oven-dried weight measurements. Mineralogy was investigated using x-ray diffraction (XRD). Quartz was the only major mineral present in the 12 samples. Albite, microcline, and albide were detected

as trace constituents in some samples. Sample physical characteristics are summarized in Table 1.

Samples were repacked in PVC sample holders for electrical measurements as a function of saturation. Coiled stainless-steel current electrodes were embedded in the samples close to the ends. Samples were first purged overnight with CO_2 in order to maximize initial saturation and then slowly saturated by through flow of pore-filling fluid. However, 100% initial saturation was not achieved. Sample saturation was varied using two procedures. First, samples (8.9-cm long, 2.5-cm diameter) were dried by progressive evaporation, achieved by opening both ends of the sample to the atmosphere. Sample saturation was determined by weighing immediately prior to an electrical measurement. Deionized water and 0.01-M NaCl electrolyte were used as pore fluids. Drying was continued until high contact resistance (>100 kΩ) at the current electrodes prevented injection of sufficient current to obtain a reliable magnitude and phase measurement with the instrumentation. In the second procedure, pressure drainage and subsequent imbibition of samples (8.9-cm long, 2.5-cm diameter) was achieved using a high-pressure syringe pump (Figure 3). Water was removed and injected from the bottom of the sample by way of a nylon membrane filter (16-psi bubble pressure). The top of the sample was open to the atmosphere via a long, narrow tube (2-mm diameter) allowing air entry but preventing evaporation. Extraction and imbibition flow rates were less than 0.5 ml/hr during both cycles. Sample saturation was determined from calculated sample porosity and precise measurement of the amount of water extracted or imbibed as recorded by the syringe pump. Large time intervals (2–3 weeks) between consecutive drainage or imbibition increments were employed to encourage pore-fluid redistribution and equilibrium prior to each electrical measurement.

RESULTS

Frequency dependence of electrical parameters

Figure 4 shows examples of the frequency dependence of the imaginary conductivity during drying. Results of evaporative

Table 1. Physical characteristics of soil samples showing grain size at which 10% of sample is finer (D_{10}), grain size distribution (Φ), porosity of repacked samples for evaporative (ϕ_{evap}) and pressure (ϕ_{press}) experiments, surface area (SSA) and real (n) and imaginary (p) saturation exponents.

Sample	D_{10} (mm)	Φ	Porosity	SSA (m^2/g)	Saturation n	Exponents p
A	0.047	1.3	0.365[1]	2.83	1.01 ± 0.15[1]	0.41 ± 0.08[1]
D	0.749	0.6	0.318[1]	0.44	1.29 ± 0.14[1]	0.61 ± 0.07[1]
			0.363[2]		1.29 ± 0.17[2]	0.80 ± 0.08[2]
			0.26[3]		2.38 ± 0.12[3]	1.43 ± 0.08[3]
E	0.071	1.9	0.313[1]	1.19	1.11 ± 0.07[1]	0.67 ± 0.05[1]
F	0.077	1.9	0.277[3]	1.76	1.23 ± 0.08[3]	0.5 ± 0.10[3]
G	0.329	1.0	0.395[3]	0.91	2.7 ± 0.09[3]	0.94 ± 0.08[3]
H	0.022	2.3	0.407[1]	1.06	2.0 ± 11[1]	1.4 ± 0.14[1]
Error[4]	±0.002	±0.1	±10%	±0.01		

[1]Evaporative drying with a 0.01-M NaCl pore fluid.
[2]Evaporative drying with a distilled water pore fluid.
[3]Pressure drainage/imbibition with a 0.01-M NaCl pore fluid.
[4]Errors calculated as follows: standard deviation for D_{10} and Φ calculated from laser particle-size results for five repeat samples, porosity relative error calculated from estimated relative error in sample volume and sample weight measurements, SSA error estimate provided by vendor, saturation exponent errors are the normal error obtained from least-square regression statistics.

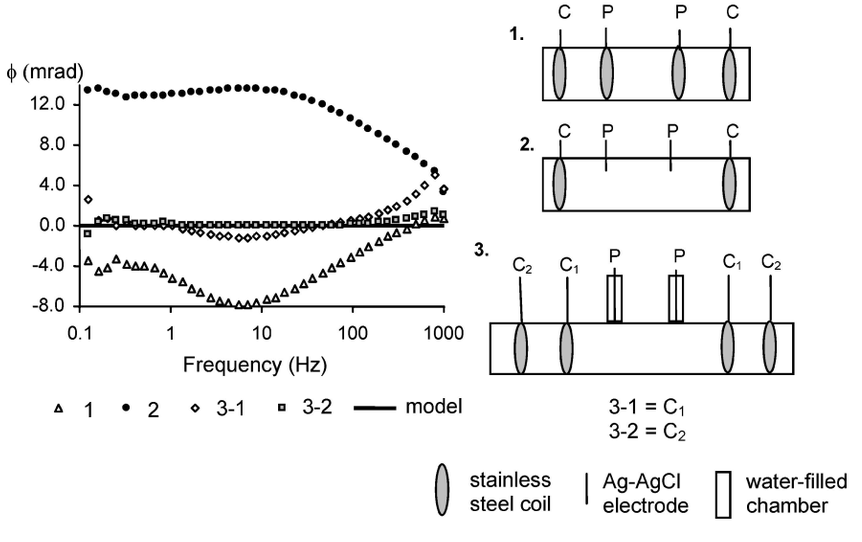

Figure 2. Measured phase as a function of Ag-AgCl potential electrode location for a 395-μS/cm water sample. (1) Coil potential electrodes placed within the sample and between the current electrodes, (2) wire electrodes extending 4 mm into the sample between the current electrodes, (3) wire electrodes placed in electrolyte-filled chambers just outside of the sample between the current electrodes, also showing the effect of distance between the current electrodes and the potential electrode pair on residual phase artifacts. The solid line shows the theoretical phase response for this sample assuming a relative dielectric permittivity of 81. "C" designates coiled current injection electrodes, and "P" designates Ag-AgCl potential electrodes. The sign convention is such that IP phase angles are positive as per equation (2).

drying for sample H are shown in Figure 4a and results of pressure drainage for sample D are shown in Figure 4b. The real conductivity (not shown) is effectively frequency independent, whereas the frequency dependence of the phase (not shown) mimics the imaginary conductivity. The imaginary conductivity of unsaturated samples dried by evaporation exhibits a weak increase with frequency and no evidence for a dominant relaxation time (length) within the measured frequency range (Figure 4a). Similar frequency dependence is commonly observed for saturated unconsolidated sediments (e.g., Börner et al., 1996; Vanhala, 1997; Slater and Lesmes, 2002). Imaginary conductivity as a function of frequency during pressure drainage exhibits a weak polarization peak for $S_w = 0.9$–0.6, suggesting the presence of a dominant relaxation length. This peak is absent for the saturated sample and for $S_w < 0.6$. It is most prominent for $S_w = 0.8$, occurring at about 8 Hz. The peak shifts slightly with changing saturation but shows no correlation with decreasing S_w. Both evaporative drying and pressure drainage results illustrate that the σ'' versus S_w relationship is frequency dependent and that S_w dependence becomes less above 100 Hz. In the following sections, we focus on the response of electrical parameters to S_w at 1 Hz, being representative of the response observed below 50 Hz and the frequency range typical of field IP data collection.

Evaporative drying

Figure 5 shows the dependence of σ', σ'', and ϕ as a function of saturation observed as samples are dried by evaporation. The real conductivity and polarization magnitude are plotted as a ratio of the value during drying to the saturated value and denoted as S' and S'', respectively. The real conductivity shows the Archie power law dependence on saturation with linear correlation coefficient (R^2) greater than 0.9 in each case. Saturation exponent (n) values are summarized in Table 1 and are at the low end of the range of values typically reported for unconsolidated sediments (Schön, 1996) but consistent with those reported in studies of similar alluvial sediments (Piggot, 1999; Baker, 2001). Similar exponents are obtained for 0.01-M NaCl saturated and distilled water saturated solutions (Figures 5d and 5e). The polarization magnitude (S'') also shows first-order power law dependence on saturation ($R^2 > 0.9$). Su et al. (2002) report a similar relationship from kilohertz-range measurements on rock during oil-driving experiments. Polarization saturation exponents (p) for our study are recorded in Table 1. Polarization-magnitude saturation exponents are consistently smaller than real-conductivity saturation exponents. There is no observable relationship between the exponents and the measured physical properties of the sediments (Table 1). The phase-angle dependence on saturation is similar for each sample with ϕ generally increasing with sample drying. Some variability is observed between samples. Above $S_w = 0.7$, the phase for sample D is only weakly saturation dependent (Figures 5d and 5e). Phase for samples A and E shows decreasing S_w dependence at lower saturation values (Figures 5a and 5b).

Pressure drainage

Figure 6 shows the dependence of σ', σ'', and ϕ as a function of saturation observed during pressure fluid extraction (denoted by subscript "ext") and subsequent fluid imbibition (denoted by subscript "imb") for samples F, D, and G. Real conductivity and polarization magnitude are normalized to values immediately prior to initiation of drainage, again denoted as S' and S'', respectively. The syringe pump allowed precise

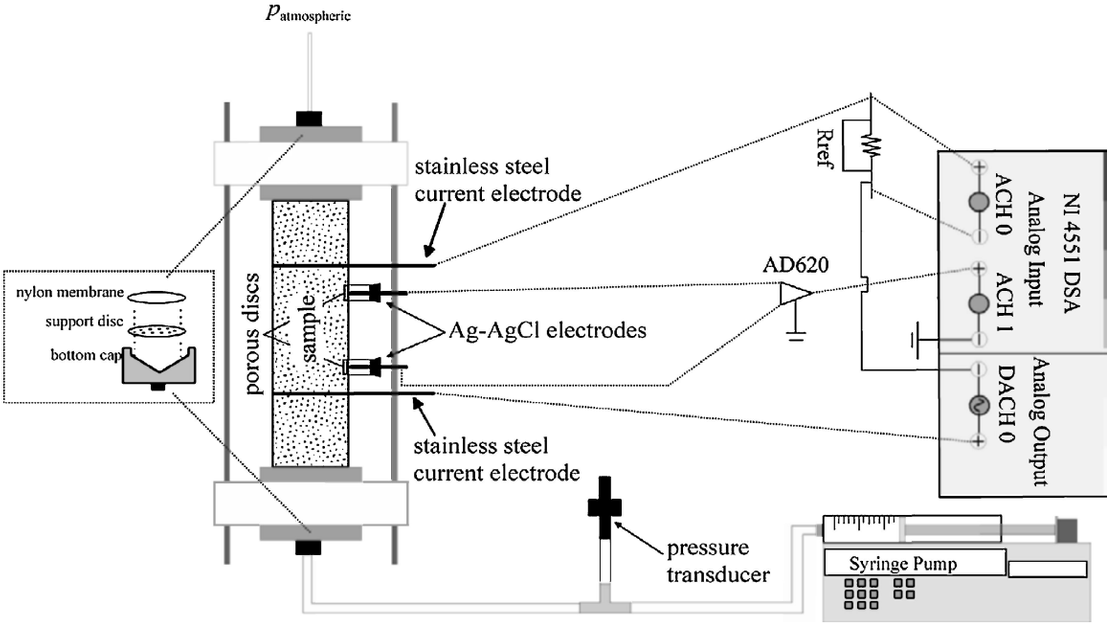

Figure 3. Schematic of sampler apparatus for IP measurements on unsaturated samples. A high-pressure syringe pump is used to induce sample drainage and imbibition. IP measurements (0.1–1000 Hz) are obtained with an NI 4551 DSA. Nonpolarizing Ag-AgCl electrodes placed in chambers just outside of the sample are kept in electrical contact with the pore fluid using high air-entry porous discs.

control of the volume of fluid removed or added, permitting a higher sampling intensity. The shape of the S' response is similar between samples. The shape of S'' during extraction is also similar between samples. The S' plots show that the saturation exponent (n) depends on saturation range and on saturation history as shown in previous work (Longeron et al., 1989; Knight, 1991). Our results show that this is also the case for the polarization magnitude as observed by Knight and Nur (1987b) at higher frequencies (30 kHz). We estimate saturation exponents for the drainage saturation interval where power law behavior is observed (Table 1). Polarization magnitude exponents are considerably smaller than real conductivity exponents, consistent with the results obtained from evaporative drying. Saturation exponents during pressure drainage of samples D and G are high relative to exponents obtained from evaporative drying. This may in part result from differences in sample preparation for the two experiments. No observable relationship between estimated exponents and sample physical properties is again observed (Table 1).

Hysteretic effects are evident in the electrical response as a function of saturation over the drainage and imbibition cycle. Hysteresis observed in the conductivity versus saturation curves is larger than that reported in other studies of unconsolidated sediments. Piggott (1999) observed minor hysteretic behavior in Ottawa sand samples, whereas Baker (2001) reported insignificant hysteretic behavior in gravels and sands. Hysteresis in our measurements is very similar to that reported for loosely consolidated sandstone and attributed to distinctly different pore-fluid distributions occurring during drainage and imbibition (Knight, 1991) as well as in more porous tuff samples (Roberts and Lin, 1997). The pore-fluid distribution at any saturation is dependent on the saturation history, sample geometry, and saturation procedure. Our experimental setup may encourage differences in pore-fluid distribution during drainage relative to during subsequent imbibition, resulting in the magnitude of hysteresis observed here.

Below $S_w \approx 0.7$, S' is lower during drainage than during subsequent imbibition. This relationship is reversed above $S_w \approx 0.7$. Real conductivity after imbibition of all extracted water is less than that at the start of drainage. We attribute this to incomplete sample saturation prior to initial drainage and redistribution of water and air in the pore space caused by the drainage-imbibition cycle. Above $S_w \approx 0.8$, there is a weak dependence of S' on saturation. In this region, extraction lowers the water level in the sample. The increased saturation dependence below $S_w \approx 0.8$ during extraction begins as water starts to drain from pores.

The polarization magnitude exhibits more complex saturation dependence although the response is very similar for the three samples and is consistent with the hysteresis observed for the dielectric constant of partially saturated sandstone at 30 kHz (Knight and Nur, 1987b). Polarization magnitude increases with S_w over some S_w intervals, yet decreases with S_w over others. This behavior is most apparent in the imbibition curves. Drainage of the water level during extraction is associated with an increase in S''. The polarization magnitude then starts to decrease as water is removed from the pores. The polarization magnitude during imbibition shows a similar shape for samples F and D but is shifted on the S_w axis. At low saturation, S'' increases with S_w during imbibition. A peak in S'' occurs at $S_w \approx 0.35$ for sample D, at $S_w \approx 0.5$ for sample F, and at $S_w \approx 0.4$ for sample G. The polarization magnitude decreases with S_w above this saturation value. Unlike samples D and F, S'' during imbibition at points exceeds the value prior to drainage. The phase response is similar for samples D and G with ϕ during extraction generally higher than during imbibition. The reverse is observed for sample F. Phase during extraction is similar to phase behavior

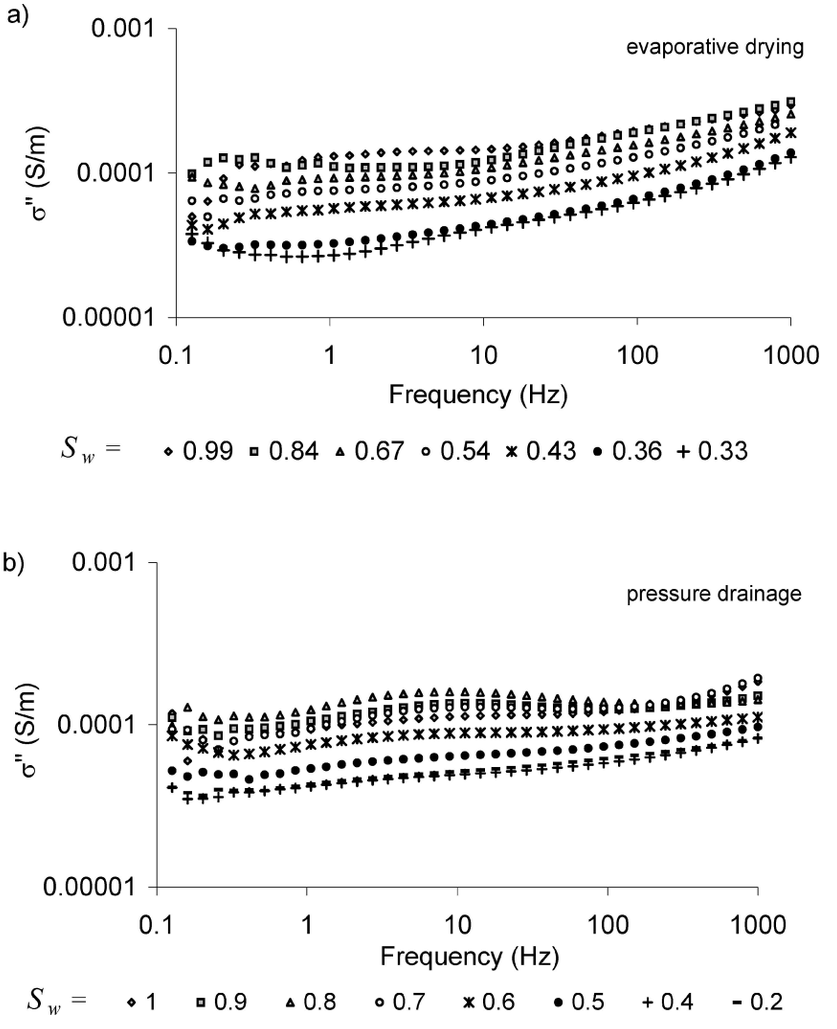

Figure 4. Examples of the frequency dependence in the imaginary conductivity spectra as a function of saturation: (a) sample H during evaporative drying, (b) sample D during pressure drainage.

during evaporative drying, exhibiting a general increase with drying.

DISCUSSION

Our results demonstrate that IP measurements are saturation dependent. Yet subsurface saturation is rarely considered in the interpretation of IP measurements. In this study, we varied saturation by both evaporative drying and by pressure drainage followed by subsequent imbibition. Electrical measurements of unsaturated laboratory samples are known to depend on the method of saturation employed (e.g., Knight, 1991). It is thus necessary to consider the degree to which our results reflect the electrical properties of the vadose zone. Evaporative drying only occurs at the earth surface, whereas the pressure drainage and imbibition employed here is somewhat similar to the pore drainage and filling that occurs when water table changes combined with capillary water removal by plants operate in the vadose zone. We did not investigate the effects of multiple drainage-imbibition cycles on electrical measurements, a process incorporated into the study of Knight (1991) and representative of the vadose zone. However, our results show that effective use of the IP method in vadose-zone studies must consider the significant effect of saturation on polarization parameters.

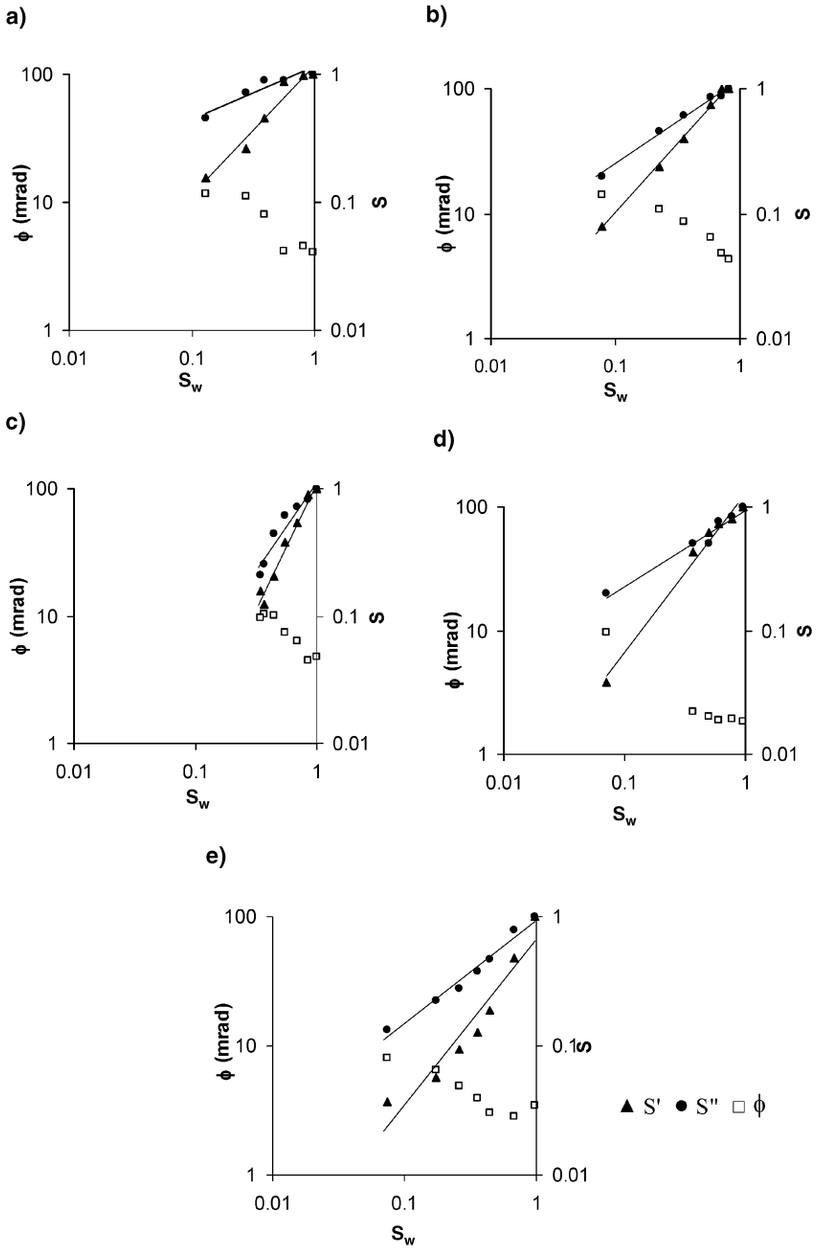

Figure 5. Dependence of real conductivity (S'), imaginary conductivity (S''), and phase angle (ϕ) on saturation (S_w) during evaporative drying of unconsolidated sediment samples initially saturated with 0.01-M NaCl (unless stated): (a) sample A, (b) sample E, (c) sample H, (d) sample D[1], (e) sample D[2] (distilled water). Real and imaginary conductivities are normalized to values at saturation. Lines show power law fits to S' and S'' ($R^2 > 0.9$) from which saturation exponents are estimated.

It is necessary in IP interpretation to distinguish between the measured parameters and the direct measures of polarization. The measured phase defines the polarization magnitude relative to the conduction magnitude [equation (2)]. Changes in the conduction term due to pore filling or drainage will cause the phase to exhibit saturation dependence even if the polarization term is constant. The phase increase during drying is largely attributed to the reduced conduction through the pore space, although changing polarization (discussed next) is also a contributing factor. Chargeability and percentage frequency effect (PFE) are measured IP parameters that will show the same character as the phase (Lesmes and Frye, 2001).

The imaginary conductivity confirms that polarization in these unconsolidated sediments is a function of saturation. However, the polarization is less affected by saturation than the conduction in both evaporative and pressure drainage experiments. In the evaporative experiments, the polarization-saturation exponents are consistently lower than the conduction-saturation exponents although there is no consistent relationship between the two. Furthermore, no obvious relationship between measured physical properties and saturation exponents was observed. Induced polarization is considered primarily sensitive to lithologic parameters (surface area, grain size, clay content) and, relative to resistivity measurements, less sensitive to the fluid chemistry. In unconsolidated sediments, the polarization shows only minor dependence on fluid chemistry, resulting in strong relationships between polarization and lithology (e.g., Slater and Glaser, 2003). Our results suggest that

these relationships are unlikely to hold in vadose zone studies in the instance of variable saturation.

We have previously noted the uncertainty regarding whether the length-scale controlling the polarization is predominantly controlled by a dominant grain size or a dominant pore size, or whether relaxations exist at both scales. Estimation of the length scale of the relaxation at the grain-fluid interface is theoretically possible (e.g., Lesmes and Morgan, 2001), but it requires values of the diffusion coefficient of the ions at this interface. We are thus unable to evaluate whether the weak relaxation peak observed is consistent with the grain-size distribution of the samples. A dependence of IP on saturation intuitively follows if the dominant relaxation mechanism is pore-size controlled. Drainage of pores and pore throats would reduce the polarization occurring at throats and pore constrictions as we observed during evaporative drying and over certain S_w intervals of a pressure-drainage cycle. As this characteristic length scale is inversely related to the pore size (Titov et al., 2002; Scott and Barker, 2003), we would expect the polarization peak in the frequency spectra to progressively shift to higher frequency (smaller pore size) as larger pores continue to drain preferentially. Spectra obtained during evaporative drying do not exhibit a polarization peak, but instead show a weak increase with frequency. Such behavior is assumed to result from the superposition of multiple relaxations over many length scales (e.g., Lesmes and Morgan, 2001), such as could result from a sample with a wide pore-size distribution. Pressure-drainage spectra do exhibit a weak polarization peak over a limited S_w range, but there is no clear correlation between the frequency of the peak and S_w. Pore-throat–dominated relaxation is likely to be more pronounced in sedimentary rocks where dissolution and cementation occur.

Chelidze and Guegen (1999) invoke a "gigantic low frequency polarization" theory, based on an EDL "open" to the bulk electrolyte, that is characterized by grain-size–controlled relaxation and appears to be consistent with saturation dependence of the IP response. In this model, polarization is enhanced by the free exchange of EDL charge with the electrolyte via ion displacement normal to the interface. Concentration gradients then build up in the electrolyte outside of the EDL. Long relaxation times result from the redistribution of charge within the electrolyte upon removal of the applied electric field. The relaxation time is grain-size controlled and a function of the bulk diffusion coefficient of the electrolyte. We suggest that removal of the electrolyte as a result of drainage would limit this polarization mechanism and result in a reduction in imaginary conductivity with drying, as generally observed in our data. In this case, the distribution of grain sizes in natural materials would result in a multitude of relaxation times and the lack of a distinct polarization peak, as observed in

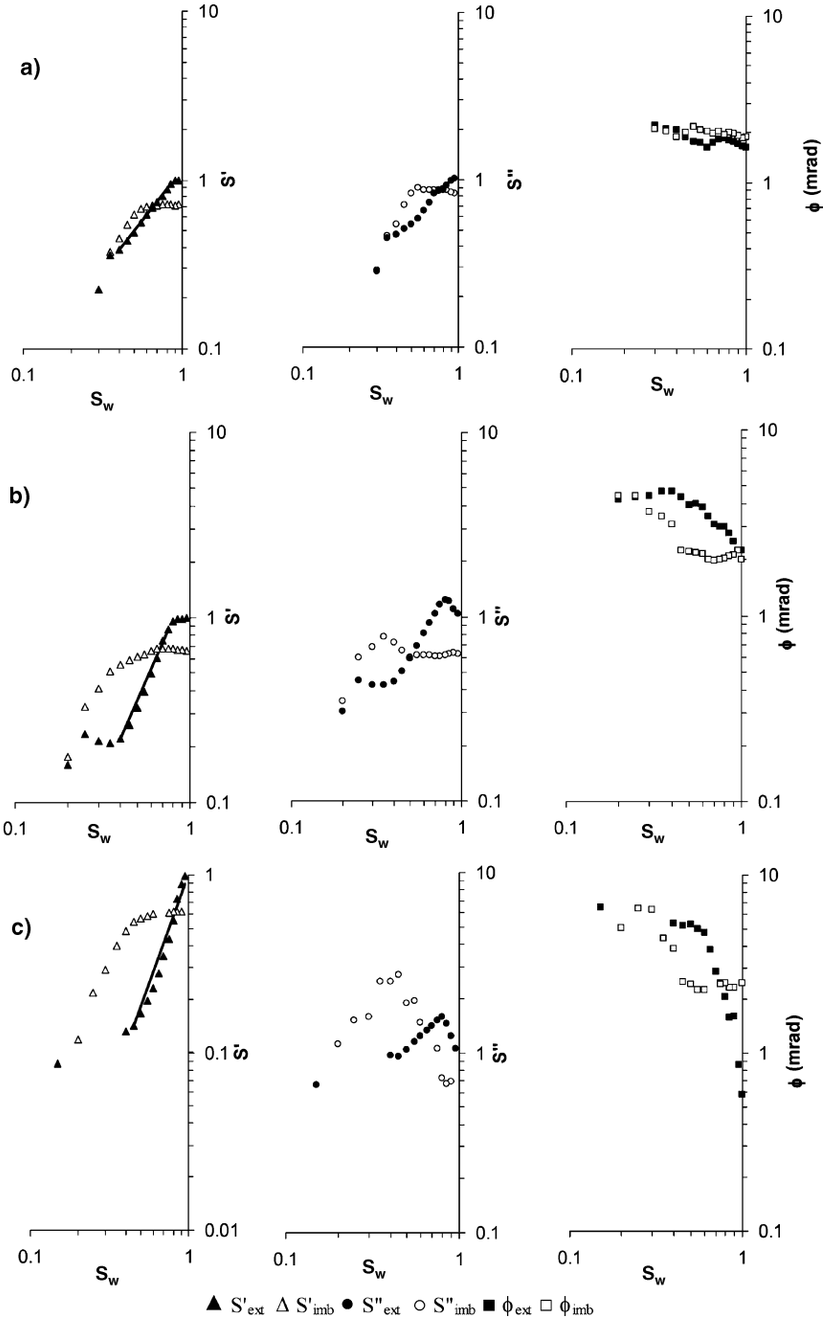

Figure 6. Real conductivity (S'), imaginary conductivity (S''), and phase (ϕ) observed at 1 Hz over a pressure drainage and subsequent imbibition cycle: (a) sample F, (b) sample D, (c) sample G. The real and imaginary conductivities are normalized to the values immediately prior to initiation of drainage. Subscripts "ext" and "imb" refer to fluid extraction (pressure drainage) and subsequent fluid imbibition, respectively.

this study. We therefore favor this grain-size–controlled model for explaining the IP saturation dependence observed during evaporative drying.

Results from the pressure-drainage experiment exhibit a complex dependence of polarization on saturation and saturation history. We cannot offer a simple explanation of these results by considering grain surface–fluid interface polarization alone. Knight (1991) proposed that surface conduction at the air-fluid interface during imbibition results from the formation of thick surface layers of water that are separated by a thin air phase (geometry B of Figure 10 in Knight, 1991). She attributed the hysteresis observed in sandstone samples as primarily resulting from this air-water interfacial conductivity being present during imbibition but absent during drainage. She cited numerous references that suggest the magnitude of the charge density at an air-water interface and resulting surface conductivity can be of the same magnitude as that occurring at the grain-fluid interface (e.g., McShea and Callaghan, 1983; Laskowski et al., 1989). If correct, it is possible that polarization at the air-fluid interface might also affect the IP response in unsaturated materials. Our real conductivity data exhibit similar hysteresis to that recorded by Knight (1991). Furthermore, our imaginary conductivity data exhibit hystereris that is very similar to that recorded at 30 kHz in partially saturated sandstone and attributed to capacitive charging and discharging of gas bubbles that is enhanced during imbibition (Knight and Nur, 1987b). This is a significant observation because it suggests that common pore-scale processes may determine the behavior of electrical properties over a wide frequency range. Due to the larger length scales controlling lower frequency polarization, we prefer to consider polarization at a continuous air-fluid interface as the most likely cause of the hysteresis observed in our IP experiments. The Knight (1991) model of surface conduction at an air-water interface assumes that a continuous air-water interface develops only during imbibition and breaks down at a S_w point when fluids rearrange to a more stable geometry ($S_w \approx 0.7$ in Knight, 1991). Figure 6 shows that the polarization during imbibition is greater than that during drainage below $S_w = 0.6$ for samples F and G, and below $S_w = 0.5$ for sample D. The effect is particularly pronounced for sample G. This polarization during imbibition exhibits a distinct maximum between $S_w = 0.4$ and $S_w = 0.5$, being most pronounced in samples D and G, and breaks down at higher saturation. Thus our results appear remarkably consistent with the Knight (1991) model.

CONCLUSIONS

IP measurements using laboratory instrumentation modified to permit measurements on unsaturated, unconsolidated samples show that IP parameters are a function of saturation (S_w), pore-fluid distribution, and saturation history. During evaporative drying, the polarization magnitude approximates power-law saturation dependence. Polarization magnitude saturation exponents (ranging between 0.4 and 1.4) are consistently less than conduction exponents (ranging between 1.1 and 2.7) for individual samples, although no clear relationship between the exponents is apparent from this study. The first-order dependence of polarization on saturation is tentatively attributed to enhancement of free exchange of EDL charge with the electrolyte via ion displacement normal to the interface, as in theory invoked by Chelidze and Guegen (1999).

Polarization measurements during pressure drainage and imbibition display a complex, yet similar between samples, saturation dependence showing clear hysteretic effects. Polarization magnitude increases with S_w over some S_w intervals, yet decreases with S_w over others, these effects being more pronounced in the imbibition curves. A distinct polarization peak develops on imbibition between $S_w = 0.35$ and $S_w = 0.5$, but is absent during pressure drainage. We propose that this enhanced polarization over a limited intermediate saturation range observed during imbibition results from the presence of a continuous charged air-fluid interface as originally suggested by Knight (1991) and previously inferred from higher frequency dielectric measurements on sandstone (Knight and Nur, 1987b). Polarization is only weakly frequency dependent over the measurement range considered here (0.1–1000 Hz), although we observe some evidence for a shift in polarization peak (relaxation time) with changing saturation.

This study shows that models describing the IP response in earth materials must consider saturation in order to predict the IP response in the vadose zone. Existing grain-surface–controlled or pore-throat–controlled relaxation models both imply a dependence of IP parameters on saturation. However, consideration of polarization at a continuous air-fluid interface is also required. Our results should encourage the development of more refined models for IP in unsaturated sediments and advance interpretation of measurements obtained within the vadose zone.

ACKNOWLEDGEMENTS

This work was supported by American Chemical Society award PRF-36265-G2. Partial support was also provided by National Science Foundation award EAR-0073680. We are grateful to University of Missouri graduate student Isaiah Utne for valuable assistance with data collection. We thank Dorthe Wildenschild (Oregon State University) for help with laboratory measurements on unsaturated sediments. David Lesmes suggested the use of porous ceramic discs as a solution to accurate IP measurements on unsaturated samples. Discussion with Andreas Kemna, Giorgio Cassiani, and Andrew Binley during a research visit to Lancaster University helped in our development of this paper. The constructive review comments provided by Rosemary Knight, two anonymous reviewers, and a *Geophysics* associate editor significantly improved the quality of this paper.

REFERENCES

Baker, K. E., 2001, Investigation of direct and indirect hydraulic property laboratory characterization methods for heterogeneous alluvial deposits: Application to the Sandria-Tech Vadose Zone infiltration site: Masters thesis, New Mexico Institute of Mining and Technology.

Börner, F. D., and Schön, J. H., 1991, A relation between the quadrature component of electrical conductivity and the specific surface area of sedimentary rocks: The Log Analyst, **32**, 612–613.

Börner, F. D., Schopper, J. R., and Weller, A., 1996, Evaluation of transport and storage properties in the soil and groundwater zone from induced polarization measurements: Geophysical Prospecting, **44**, 583–602.

Chelidze, T. L., and Gueguen, Y., 1999, Electrical spectroscopy of porous rocks: a review—I. Theoretical models: Geophysical Journal International, **137**, 1–15.

Garrouch, A. A., 1999, Systematic study revealing resistivity dispersion in porous media: The Log Analyst, **40**, 271–279.

Kemna, A., 2000, Tomographic inversion of complex resistivity—Theory and application: Der Andere Verlag.

Klein, J. D., and Sill, W. R., 1982, Electrical properties of artificial clay-bearing sandstones: Geophysics, **47**, 1593–1605.
Knight, R., 1991, Hysteresis in the electrical resistivity of partially saturated sandstones: Geophysics, **56**, 2139–2147.
Knight, R., and Endres, A., 2003, Introduction to rock physics for near-surface aplications in near-surface geophysics, **1**, SEG, in press.
Knight, R. J., and Nur, A., 1987a, The dielectric constant of sandstones, 60 kHz to 4 MHz: Geophysics, **52**, 644–654.
——— 1987b, Geometrical effects in the dielectric response of partially saturated sandstones, The Log Analyst, **28**, 513–519.
Laskowski, J. S., Yordan, J. L., and Yoon, R. H., 1989, Electrokinetic potentials of microbubbles generated in aqueous solutions of weak electrolyte type surfactants: Langmuir, **5**, 373–376.
Lesmes, D. P., 1993, Electrical-impedance spectroscopy of sedimentary rocks: Ph.D. dissertation, Texas A&M University.
Lesmes, D. P., and Frye, K. M., 2001, The influence of pore fluid chemistry on the complex conductivity and induced-polarization responses of Berea sandstone: Journal of Geophysical Research, **106**, B3, 4079–4090.
Lesmes, D. P., and Morgan, F. D., 2001, Dielectric spectroscopy of sedimentary rocks: Journal of Geophysical Research, **106**, B7, 13 329–13 346.
Lima, O. A. L., and Niwas, S., 2000, Estimation of hydraulic parameters of shaly sandstone aquifers from geoelectrical measurements: Journal of Hydrology, **235**, 12–26.
Lima, O. A. L., and Sharma, M. M., 1992, A generalized Maxwell-Wagner theory for membrane polarization in shaly sands: Geophysics, **57**, 431–440.
Longeron, D. G., Argaud, M. J., and Feraud, J. P., 1989, Effect of overburden pressure and the nature and microscopic distribution of fluids on electrical properties of rock samples: SPE Formation Evaluation, **4**, June, 194–201.
McShea, J. A., and Callaghan, I. C., 1983, Electrokinetic potentials at the gas-aqueous interface by spinning cylinder electrophoresis: Colloid Polymer Science, **261**, 757–766
Piggott, S. D., 1999, Saturation history effects on the electrical properties of Ottawa sand during water-air and water-LNAPL drainage-imbibition experiments: Master's thesis, University of Waterloo.
Revil, A., and Glover, P. W. J., 1998, Nature of surface electrical conductivity in natural sands, sandstones, and clays: Geophysical Research Letters, **25**, 691–694.
Roberts, J. J., and Lin, W., 1997, Electrical properties of partially saturated Topopah Spring tuff: Water distribution as a function of saturation: Water Resources Research, **33**, 577–587.
Schön, J. H., 1996, Physical properties of rocks—Fundamentals and principles of petrophysics: Peramon Press.
Schopper, J. R., Kulenkampff, J. M., and Debschütz, W. G., 1997, Grenzflächenleitfähigkeit, *in* Knödel, K., Krummel, H., and Lange, G., eds., Handbuch zur Erkundung des Untergrundes von Deponien und Altasten, Band 3—Geophysik: Springer-Verlag, 992–995.
Scott, J. B. T., and Barker, R. D., 2003, Determining throat size in Permo-Triassic sandstones from low frequency electrical spectroscopy: Geophysical Research Letters, **30**, GL012951
Slater, L., and Glaser, D. R., 2003, Controls on induced polarization in sandy unconsolidated sediments and application to aquifer characterization: Geophysics, **68**, 1547–1558.
Slater, L., and Lesmes, D. P., 2002, Elected-hydraulic relationships observed for unconsolidated sediments: Water Resources Research, **38**, No. 10, 31-1 to 31-10.
Su, Q., Feng, Q., and Shang, Z., 2000, Electrical impedance variation with water saturation in rock: Geophysics, **65**, 68–75.
Titov, K., Komarov, V., Tarasov, V., and Levitski, A., 2002, Theoretical and experimental study of time domain-induced polarization in water-saturated sands: Journal of Applied Geophysics, **50**, 4, 417–433.
Vanhala, H., 1997, Mapping oil contaminated sand and till with the spectral induced polarization method: Geophysical Prospecting, **45**, 303–326.
Vanhala, H., and Soininen, H., 1995, Laboratory technique for measurement of spectral induced polarization response of soil samples: Geophysical Prospecting, **43**, 655–676.
Vinegar, H. J., and Waxman, M. H., 1984, Induced polarization of shaly sands: Geophysics, **49**, 1267–1287.
Ward, S. H., 1990, Resistivity and induced polarization methods, *in* Ward, S. H. ed., Geotechnical and environmental geophysics: SEG, 169–189.
Waxman, M. H., and Smits, L. J. M., 1968, Electrical conductivities in oil-bearing shaly sands: Society of Petroleum Engineers Journal, **243**, 107–122.
Worthington, P. F., and Collar, F. A., 1984, Relevance of induced polarization to quantitative formation evaluation: Marine and Petroleum Geology, **1**, 14–26.